Langmuir
Article
pubs.acs.org/Langmuir

Anthraquinone-Based Discotic Liquid Crystals

Amy E. Murschell and Todd C. Sutherland*

Department of Chemistry, University of Calgary, 2500 University Drive NW, Calgary, Alberta, Canada

Received April 8, 2010. Revised Manuscript Received June 8, 2010

The syntheses of six room-temperature discotic liquid crystals based on an alkoxy-anthraquinone (AQ) framework is described. Differential scanning calorimetry, X-ray diffraction (XRD), and cross-polarized microscopy were used to identify phases and confirm phase-transition temperatures. Cross-polarized microscopy results suggest columnar discotic structures at room temperature. However, the AQ derivatives also undergo mesophase-to-mesophase transitions, which are attributed to rectangular- to hexagonal-columnar discotic transitions based on XRD analysis. Furthermore, some of the compounds display remarkable liquid crystalline phase stability that spans from −50 to 150 °C, a useful temperature range for organic materials applications. The different AQ derivatives did not exhibit electronic perturbations, as all compounds have absorption onsets of approximately 400 nm. Finally, solution cyclic voltammetry of the AQ derivatives was carried out to determine the redox potentials, diffusion coefficients, and electron transfer rate constants. All AQ derivatives had $E_{1/2}$ values that ranged between −1.52 and −1.70 V vs Fc/Fc^+. Diffusion coefficients and electron transfer rates for all AQ derivatives ranged between 0.4 and 7.1×10^{-6} $cm^2 \cdot s^{-1}$ and 0.9 and 5.2×10^{-3} $cm \cdot s^{-1}$, respectively.

Introduction

Anthraquinones (AQs) are critical components to the development of a variety applications, such as the dye industry,[1] drug synthesis,[2] and organic materials.[3,4] Chemically related quinones are key components of both respiration and photosynthesis because of their inherent proton-coupled redox properties.[5] The redox reactions of quinones, although seemingly simple reactions, are still an active area of research because of the $2H^+$ and $2e^-$ reactions.[6,7] The AQ framework represents a simple scaffold for which numerous covalent modifications are possible. Owing to the synthetic versatility of AQs and the known two-electron transfer reactions, this contribution explores alkylation reactions of hexahydroxy-AQs for the purpose of forming discotic liquid crystals (DLCs) that may lead to new organic materials that carry charges efficiently.

DLCs are a mesophase that is often observed with rigid planar molecules bearing several pendant long alkyl chains.[8−14] The planar molecules typically consist of triphenylene,[15−19] phthalocyanines,[20−23] perylene diimide,[24−27] hexabenzocoronene[28−31] and anthraquinones.[32−35] We chose to modify AQ because of the stable redox properties that could be exploited in designing organic materials that could display charge transport properties. In addition, there are numerous reports of DLCs that are based on the AQ core, rufigallol (1,2,3,5,6,7-hexahydroxy-AQ).[36−43]

*To whom correspondence should be addressed. E-mail: todd.sutherland@ucalgary.ca. Fax: 01 403 289 9488. Tel.: 01 403 220 7559.

(1) Ferreira, E. S. B.; Hulme, A. N.; McNab, H.; Quye, A. *Chem. Soc. Rev.* **2004**, *33*, 329–336.
(2) Maier, M. E.; Bosse, F.; Niestroj, A. J. *Eur. J. Org. Chem.* **1999**, *1999*, 1–13.
(3) Catellani, M.; Luzzati, S.; Lupsac, N.-O.; Mendichi, R.; Consonni, R.; Famulari, A.; Meille, S. V.; Giacalone, F.; Segura, J. L.; Martin, N. *J. Mater. Chem.* **2004**, *14*, 67–74.
(4) Mamada, M.; Nishida, J.-i.; Tokito, S.; Yamashita, Y. *Chem. Commun.* **2009**, 2177–2179.
(5) Hillard, E. A.; Abreu, F. C. d.; Ferreira, D. C. M.; Jaouen, G.; Goulart, M. O. F.; Amatore, C. *Chem. Commun.* **2008**, 2612–2628.
(6) Concepcion, J. J.; Brennaman, M. K.; Deyton, J. R.; Lebedeva, N. V.; Forbes, M. D. E.; Papanikolas, J. M.; Meyer, T. J. *J. Am. Chem. Soc.* **2007**, *129*, 6968–6969.
(7) Trammell, S. A.; Lebedev, N. *J. Electroanal. Chem.* **2009**, *632*, 127–132.
(8) Chandrasekhar, S. *Liq. Cryst.* **1993**, *14*, 3–14.
(9) Chenard, Y.; Paiement, N.; Zhao, Y. *Liq. Cryst.* **2000**, *27*, 459–465.
(10) Ciferri, A. *Liq. Cryst.* **2004**, *31*, 1487–1493.
(11) Grimsdale, A. C.; Wu, J.; Muellen, K. *Chem. Commun.* **2005**, 2197–2204.
(12) Kumar, S. *Chem. Soc. Rev.* **2006**, *35*, 83–109.
(13) Laschat, S.; Baro, A.; Steinke, N.; Giesselmann, F.; Haegele, C.; Scalia, G.; Judele, R.; Kapatsina, E.; Sauer, S.; Schreivogel, A.; Tosoni, M. *Angew. Chem., Int. Ed.* **2007**, *46*, 4832–4887.
(14) Sergeyev, S.; Pisula, W.; Geerts, Y. H. *Chem. Soc. Rev.* **2007**, *36*, 1902–1929.
(15) Markovitsi, D.; Lecuyer, I.; Lianos, P.; Malthete, J. *J. Chem. Soc., Faraday Trans.* **1991**, *87*, 1785–1790.
(16) Boden, N.; Borner, R. C.; Bushby, R. J.; Cammidge, A. N.; Jesudason, M. V. *Liq. Cryst.* **1993**, *15*, 851–858.
(17) vandeCraats, A. M.; Warman, J. M.; deHaas, M. P.; Adam, D.; Simmerer, J.; Haarer, D.; Schuhmacher, P., *Adv. Mater.* **1996**, *8*, 823-&.
(18) van de Craats, A. M.; Siebbeles, L. D. A.; Bleyl, I.; Haarer, D.; Berlin, Y. A.; Zharikov, A. A.; Warman, J. M. *J. Phys. Chem. B* **1998**, *102*, 9625–9634.
(19) Kumar, S. *Liq. Cryst.* **2004**, *31*, 1037–1059.
(20) Masurel, D.; Sirlin, C.; Simon, J. *New J. Chem.* **1987**, *11*, 455–456.
(21) Cook, M. J. *J. Mater. Chem.* **1996**, *6*, 677–689.
(22) Zhou, R.; Josse, F.; Gopel, W.; Ozturk, Z. Z.; Bekaroglu, O. *Appl. Organomet. Chem.* **1996**, *10*, 557–577.
(23) Fox, J. M.; Katz, T. J.; Van Elshocht, S.; Verbiest, T.; Kauranen, M.; Persoons, A.; Thongpanchang, T.; Krauss, T.; Brus, L. *J. Am. Chem. Soc.* **1999**, *121*, 3453–3459.
(24) Gregg, B. A.; Cormier, R. A. *J. Phys. Chem. B* **1998**, *102*, 9952–9957.
(25) Gregg, B. A.; Cormier, R. A. *J. Am. Chem. Soc.* **2001**, *123*, 7959–7960.
(26) Liu, S. G.; Sui, G. D.; Cormier, R. A.; Leblanc, R. M.; Gregg, B. A. *J. Phys. Chem. B* **2002**, *106*, 1307–1315.
(27) Schmidt-Mende, L.; Watson, M.; Mullen, K.; Friend, R. H. *Mol. Cryst. Liq. Cryst.* **2003**, *396*, 73–90.
(28) Muller, M.; Kubel, C.; Mullen, K. *Chem.—Eur. J.* **1998**, *4*, 2099–2109.
(29) Schmidt-Mende, L.; Fechtenkotter, A.; Mullen, K.; Moons, E.; Friend, R. H.; MacKenzie, J. D. *Science* **2001**, *293*, 1119–1122.
(30) Fischbach, I.; Pakula, T.; Minkin, P.; Fechtenkotter, A.; Mullen, K.; Spiess, H. W.; Saalwachter, K. *J. Phys. Chem. B* **2002**, *106*, 6408–6418.
(31) Simpson, C. D.; Wu, J. S.; Watson, M. D.; Mullen, K. *J. Mater. Chem.* **2004**, *14*, 494–504.
(32) Werth, M.; Leisen, J.; Boeffel, C.; Dong, R. Y.; Spiess, H. W. *J. Phys. II* **1993**, *3*, 53–67.
(33) Krishnan, K.; Balagurusamy, V. S. K. *Liq. Cryst.* **2000**, *27*, 991–994.
(34) Prasad, V.; Rao, D. S. S., *Mol. Cryst. Liq. Cryst.* **2000**, *350*, 51-+.
(35) Krishnan, K.; Balagurusamy, V. S. K. *Liq. Cryst.* **2001**, *28*, 321–325.
(36) Billard, J.; Dubois, J. C.; Vaucher, C.; Levelut, A. M. *Mol. Cryst. Liq. Cryst.* **1981**, *66*, 435–442.
(37) Carfagna, C.; Iannelli, P.; Roviello, A.; Sirigu, A. *Liq. Cryst.* **1987**, *2*, 611–616.
(38) Raja, K. S.; Ramakrishnan, S.; Raghunathan, V. A. *Chem. Mater.* **1997**, *9*, 1630–1637.
(39) Raja, K. S.; Raghunathan, V. A.; Ramakrishnan, S. *Macromolecules* **1998**, *31*, 3807–3814.
(40) Dvinskikh, S. V.; Luz, Z.; Zimmermann, H.; Maliniak, A.; Sandstroem, D. *J. Phys. Chem. B* **2003**, *107*, 1969–1976.
(41) Kumar, S.; Naidu, J. J.; Varshney, S. K. *Liq. Cryst.* **2003**, *30*, 319–323.
(42) Maeda, Y.; Yokoyama, H.; Kumar, S. *Liq. Cryst.* **2005**, *32*, 833–845.
(43) Bisoyi, H. K.; Kumar, S. *Tetrahedron Lett.* **2007**, *48*, 4399–4402.

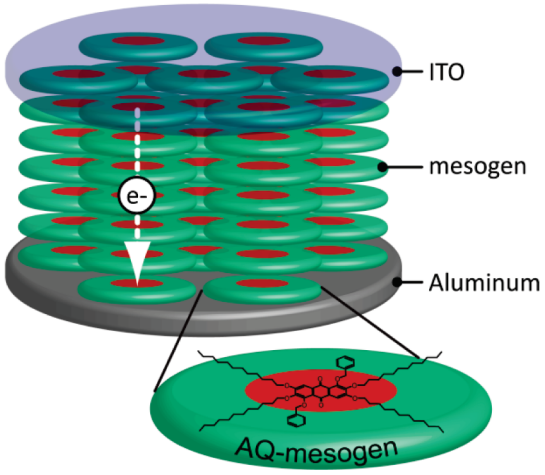

Figure 1. Schematic of DLC consisting of anthraquinone mesogens that are sandwiched between two electrodes, indium tin oxide (ITO) and aluminum.

The majority of DLCs consist of an extended aromatic core that contains two or more alkyl chains to form disk-shaped mesogens. DLCs are unique because of the long-range ordering into stacks of discs forming columns. These columns force aromatic cores to overlap, while the long alkyl chains maintain fluidity and LC properties. Typically, the aromatic core-to-core separation distance is small at 3−3.5 Å, which should allow for efficient one-dimensional migration of charge. Importantly, the charges should migrate through the stacks with minimal hopping between stacks because of the large distance between columns. Because of the effective pi-conduit, it is enticing to use DLCs for organic materials applications involving charge transport, such as organic light-emitting diodes, organic field-effect transistors, or organic photovoltaic cells. Figure 1 illustrates the model packing of columnar hexagonal DLC that could be placed between electrodes and used as a conducting organic material under potential bias. The idealized functional form, shown in Figure 1, illustrates the overlap of pi-electrons of the anthraquinones cores and efficient shuttling of electrons through the pi-electron conduit, which is insulated from neighboring columns by long alkyl chains. AQs are expected to be useful in devices because the redox reactions are generally reversible with stabilized radical anion intermediates, which should lead to long-term stability in devices. DLC structures offer numerous advantages over other organic charge carriers. For example, DLCs are formed spontaneously by a self-assembly process. The self-assembly is critical because it allows the formation of large area films by simple solution deposition techniques. Compared to conducting polymers where charges migrate in a random walk by hopping from site to site, the organized structure of DLCs allows for more efficient charge migration.[18] A consequence of the hopping mechanism used in polymeric materials to carry charge is a higher probability of charge recombination (hole + electron) leading to less than ideal charge mobility. Polymeric materials suffer from polydispersity, whereas DLCs are made of discrete structures that can be analytically purified and characterized leading to more insightful structure−function relationships. In addition, the organized structure of DLCs spans a useful dimension scale from molecular to several micrometers, permitting device fabrication with conventional electrodes.[14] With all organic materials that carry charge, over time the material will degrade, but DLCs offer the opportunity to renew the supramolecular structure when they are heated above the isotropic temperature. Because DLCs consist of discrete molecules, electronic tuning of the charge carrying components should be easier than polymeric materials because secondary structures, such as microcrystalline domains that can have dramatic effects on performance, are absent.

Conceptually, DLCs offer promising potential for efficient organic charge transport as several authors have previously reported.[44−52] This contribution outlines the synthesis of a class of AQ DLCs that have the potential to operate as *n*-type material in carrying electrons under applied potentials. There are limited examples of organic compounds that transport electrons (*n*-type requirement), such as BTD (benzothiadiazole), perylene bisimide, and PCBM (phenyl-C_{61}-butyric acid methyl ester), and AQs offer an additional compound class to this small family. Much successful research has been conducted on *p*-type materials, such as polythiophenes, which show excellent hole transport properties. Previous reports of AQ liquid crystals have shown promising self-organization properties, such as columns that extend to the nanometer range but possess limited room temperature liquid crystalline characteristics. There is only one report of an AQ liquid crystal that explores benzyloxy substituents at the 1,5-AQ positions. This work explores the effects of electronically different aryl derivatives in the 1,5-AQ positions, which play important roles in both the self-assembling, long-range columnar ordering and thermal stability. Furthermore, previous AQ liquid crystal reports do not explore the complex electrochemistry of quinones, which will have consequences on their charge carrying capacity. The compounds are characterized with conventional organic techniques and the electronic properties were assessed by UV−vis absorption spectroscopy and cyclic voltammetry. The DLC properties were assessed by differential scanning calorimetry (DSC), cross-polarized microscopy, and X-ray diffraction (XRD) studies.

Results and Discussion

The synthesis of all hexaether-anthraquninones begins with the microwave-assisted self-condensation of gallic acid in concentrated sulfuric acid, shown in Scheme 1, following the work of Bisoyi and Kumar.[43] The self-condensation product, ruffigalol, **1**, was purified by crystallization to give isolated yields of 84%. Rufigallol was treated with base at 85 °C and dodecylbromide was added to produce the 2,3,6,7-tetradodecyl anthraquinone (AQ) **2** in 80% yield, which was purified by precipitation and rinsing. It was found that addition of the phase transfer catalyst (tetrabutylammonium bromide, TBAB) increased the rate of the tetra alkylation, and using stoichiometric amounts of the alkylbromide led exclusively to the tetra-alkylated product. The formation of the tetra-alkylated-AQ is confirmed by the presence

(44) An, Z. Z.; Yu, J. S.; Domercq, B.; Jones, S. C.; Barlow, S.; Kippelen, B.; Marder, S. R. *J. Mater. Chem.* **2009**, *19*, 6688–6698.
(45) Feng, X. L.; Marcon, V.; Pisula, W.; Hansen, M. R.; Kirkpatrick, J.; Grozema, F.; Andrienko, D.; Kremer, K.; Mullen, K. *Nat. Mater.* **2009**, *8*, 421–426.
(46) Marcon, V.; Breiby, D. W.; Pisula, W.; Dahl, J.; Kirkpatrick, J.; Patwardhan, S.; Grozema, F.; Andrienko, D. *J. Am. Chem. Soc.* **2009**, *131*, 11426–11432.
(47) Miyake, Y.; Fujii, A.; Ozaki, M.; Shimizu, Y. *Synth. Met.* **2009**, *159*, 875–879.
(48) Pisula, W.; Zorn, M.; Chang, J. Y.; Mullen, K.; Zentel, R. *Macromol. Rapid Commun.* **2009**, *30*, 1179–1202.
(49) Schouten, P. G.; Warman, J. M.; Dehaas, M. P.; Vannostrum, C. F.; Gelinck, G. H.; Nolte, R. J. M.; Copyn, M. J.; Zwikker, J. W.; Engel, M. K.; Hanack, M.; Chang, Y. H.; Ford, W. T. *J. Am. Chem. Soc.* **1994**, *116*, 6880–6894.
(50) Simmerer, J.; Glusen, B.; Paulus, W.; Kettner, A.; Schuhmacher, P.; Adam, D.; Etzbach, K. H.; Siemensmeyer, K.; Wendorff, J. H.; Ringsdorf, H.; Haarer, D., *Adv. Mater.* **1996**, *8*, 815+.
(51) Struijk, C. W.; Sieval, A. B.; Dakhorst, J. E. J.; van Dijk, M.; Kimkes, P.; Koehorst, R. B. M.; Donker, H.; Schaafsma, T. J.; Picken, S. J.; van de Craats, A. M.; Warman, J. M.; Zuilhof, H.; Sudholter, E. J. R. *J. Am. Chem. Soc.* **2000**, *122*, 11057–11066.
(52) van de Craats, A. M.; Warman, J. M.; Fechtenkotter, A.; Brand, J. D.; Harbison, M. A.; Mullen, K. *Adv. Mater.* **1999**, *11*, 1469–1472.

Scheme 1. Synthesis of Hexaether-anthraquinones

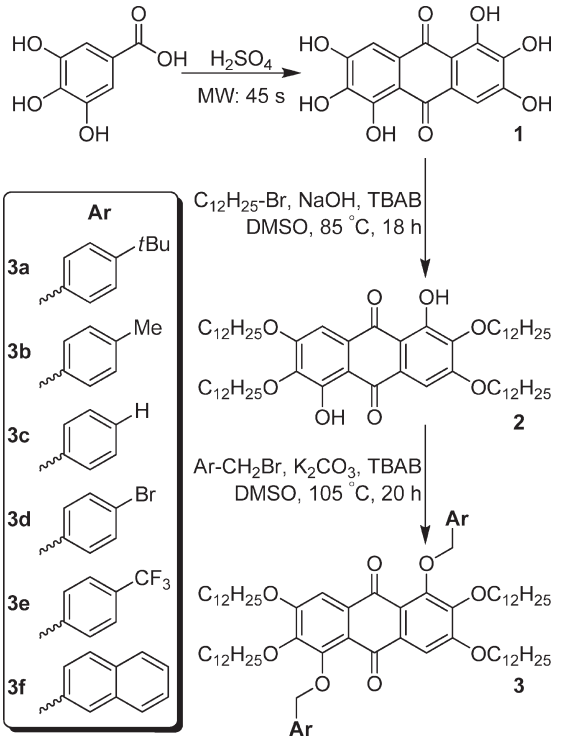

of the diagnostic downfield H-bonded 1,5-dihydroxyl protons at 12.78 ppm in the ^{1}H NMR. Compound **2** was further dialkylated with the appropriate benzyl bromide derivative to produce compounds **3a**−**f**. Although the conditions were less basic than the previous step, a higher temperature was needed to react the deactivated 1,5-phenoxide nucleophiles. Again, a phase transfer catalyst was found to increase the rate of formation of **3**. Similar analogues of **3** have been shown to display liquid crystalline properties and series **3a** to **3f** were synthesized to assess the electronic and/or shape parameters involved in solid-state packing.

The electronic perturbation of the 1,5-dibenzyl derivatives (**3a**−**f**) were assessed by UV−vis spectroscopy, included in the Supporting Information. As anticipated, negligible differences in the absorption profiles are seen for all compounds, suggesting the 1,5-dialkoxy substitutions exert little electronic effect on either the HOMO or LUMO orbitals. Because of the interruption in conjugation between the AQ and the benzyl groups, little orbital mixing was predicted, but the intermolecular electronic effects ($\pi-\pi$ interactions) in the solid-state were unknown. The exception is the dinaphthyl derivative (**3f**) which shows a larger molar absorptivity at high energy, which is attributed to the naphthalene behaving as an independent chromophore, as compared to the phenyl chromophores in **3a**−**e**.

Figure 2 shows digital images of films of **3d** and **3e** on glass microscope slides under a cross-polarized light microscope at room temperature. The films were formed by placing the compounds on a clean glass microscope slide and heating the slide above isotropic liquid temperature (170 °C) on a hot plate for 5 min then cooling to room temperature by removing the slide from the hot plate. The cross-polarized images (40× magnification) of films of **3d** and **3e** show conic focal patterns,[53] which is typical of discotic liquid crystalline phases. All compounds synthesized display discotic mesophase properties at room temperature because under stress or sheer the phases change, which indicates the quasi-liquid properties are maintained. The dark portions of the figure represent areas where the film formation did not occur since the compounds do not flow well on a hydrophilic glass surface. Both film samples were also annealed at 120 °C in an oven for 24 h and the domains grew larger, indicating long-range order of the LC domains occurs slowly.

X-ray diffraction (XRD) studies were carried out on anthraquinones **3a**−**f** and the analysis is shown in table 1 and the selected diffraction data are shown in Figure 3a. Three regions are broadly defined to interpret the patterns. First, the low angle region between 2° and 10° 2θ degrees is useful to index the two-dimensional lattice. Second, the very broad peak between 17° and 23° 2θ degrees highlighted in red, which is most evident in **3c**, is characteristic of the liquid-like state of the long alkyl chains. Finally, the peak highlighted in blue on Figure 3a, is indicative of the aromatic core-to-core distance, which is typically more crystalline than the alkyl region leading to a sharper peak. The width of the core-to-core peak in XRD can be used as a measure of correlation length, or crystalline domain size using the Scherrer formula.[54] Samples for XRD analysis were prepared by placing the compound on a clean glass slide and heating the slide to 170 °C, where all materials enter the isotropic phase, then cooled to room temperature and mounted. The LC samples were placed onto plastic sample holders for the XRD instrument, and the glass slide and polymer sample tray were collected as background diffraction patterns and are included in the Supporting Information. Note, all of the XRD experiments were conducted at room temperature. The plastic sample tray contains peaks that are shown as the four vertical dashed lines in Figure 3a, and due to the overlap of the sample tray signals with the alkyl region a quantitative peak assignment is not possible. Qualitatively, the peak in the alkyl region is broad and consistent with liquid-like characteristics. In the high angle region, there is a broad peak between 25 and 26 θ degrees for compounds **3a**−**d** and **3f**. This high angle peak corresponds to a *d*-spacing of approximately 3.4 Å, which suggests the core-to-core distance between anthraquinones is small and compares well with related compounds.[55−57] The low angle peaks in the XRD divide the compounds into two types of lattices.

Anthraquinones **3b**, **3c,** and **3e** have peaks that are consistent with hexagonal columnar structures due to the ratio of the *d*-spacing as $1:1/\sqrt{3}:1/2:1/\sqrt{7}$ that are indexed to the 10, 11, 20, and 21 reflections, respectively, in a 2-dimensional lattice.[58] Furthermore, similar compounds have also shown a hexagonal columnar (Col_h) phase.[55−59] Conversely, compounds **3a**, **3d**, and **3f** do not exhibit the simple hexagonal columnar *d*-spacing ratios but do show peaks consistent with a rectangular columnar (Col_r) structure. The indices are indicated for all compounds in Figure 3a and in the XRD summary Table 1.

Both the XRD data and cross-polarized microscopy images were taken at room temperature, and a critical property of liquid crystals is their thermal behavior as assessed by differential scanning calorimetry (DSC), shown in Figure 3b.

(53) Chandrasekhar, S. *Liquid Crystals*, 2nd ed.; Cambridge University Press: Cambridge England; New York, 1992; p xv, 460.

(54) Will, G. *Powder diffraction: The Rietveld Method and the Two-Stage Method to Determine and Refine Crystal Structures from Powder Diffraction Data*; Springer: Berlin; New York, 2006; p ix, 224.

(55) Blanton, T. N.; Chen, H. P.; Mastrangelo, J.; Chen, S. H. *Adv. X-Ray Anal.* **2001**, *44*, 18–23.

(56) Sun, Z.; Wang, H.; Qiu, D.; Wang, L. *Phys. Status Solidi A* **1987**, *101*, K93–K96.

(57) Krishnan, K.; Balagurusamy, V. S. K. *Mol. Cryst. Liq. Cryst. Sci. Technol., Sect. A* **2000**, *350*, 1–18.

(58) Prasad, S. K.; Rao, D. S. S.; Chandrasekhar, S.; Kumar, S. *Mol. Cryst. Liq. Cryst.* **2003**, *396*, 121–139.

(59) Prasad, V.; Krishnan, K.; Balagurusamy, V. S. K. *Liq. Cryst.* **2000**, *27*, 1075–1085.

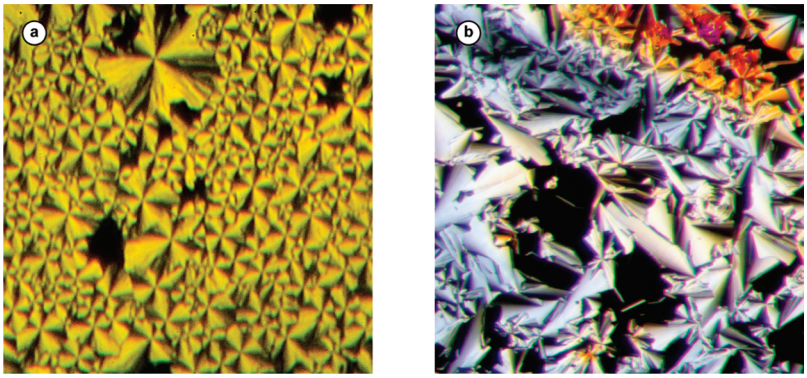

Figure 2. Cross-polarized microscope images of (a) **3d** and (b) **3e** at 40× magnification.

Table 1. X-ray Diffraction Data for Films of 3a−f on Glass at Room Temperature

	d-spacing (Å) (index)				lattice parameters (Å)		
	peak 1	peak 2	peak 3	core−core (Å)	*a*	*b*	correlation length (Å)
3a	23.7 (110)	20.8 (020)	13.5 (230)	3.42	41.6	28.9	188
3b	21.0 (100)	12.4 (110)	10.8 (200)	3.40	24.3		188
3c	22.4 (100)	13.1 (110)	11.3 (200)	3.44	25.9		161
3d	27.1 (110)	21.1 (020)	18.0 (230)	3.41	42.2	35.1	181
3e	23.1 (100)	14.0 (110)	12.0 (200)	3.78	26.7		N/A[a]
3f	27.4 (110)	19.1 (020)	14.2 (230)	3.41	38.2	38.2	191

[a] N/A = not available.

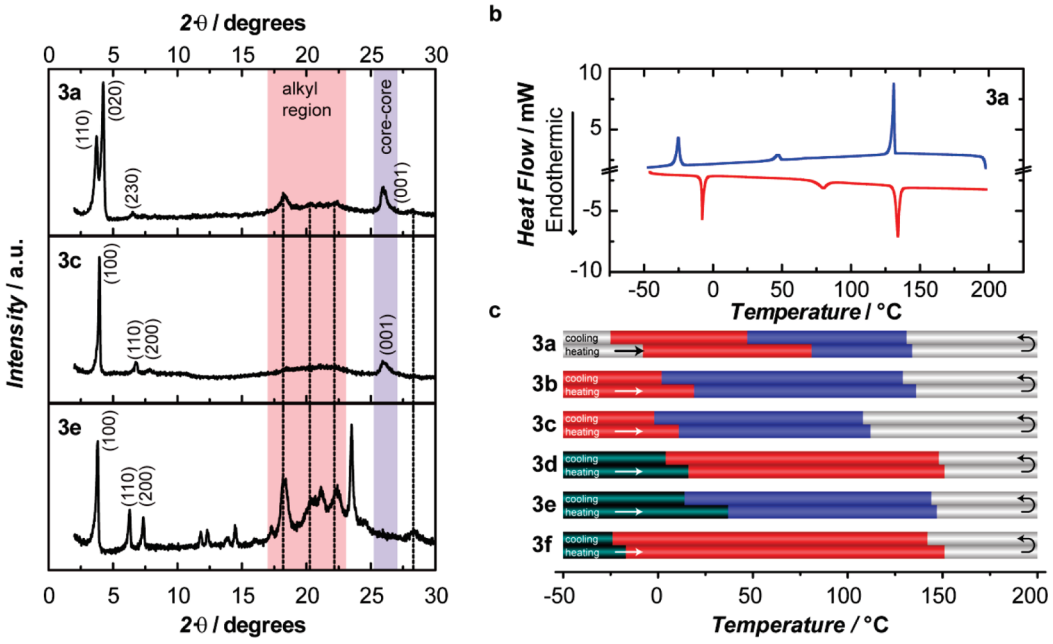

Figure 3. (a) X-ray diffraction patterns for **3a**, **3c**, and **3e**. The dashed lines are peaks attributed to the sample holder. (b) DSC trace of the heating (red) and cooling (blue) traces (10 °C·min^{-1}) of **3a**. (b) Summary of the phase transitions upon heating and cooling of compounds **3a**−**f**; red bars are assigned to the Col_r phase, blue bars are assigned to the Col_h phase, black bars are an unassigned phase.

A DSC for anthraquinone **3a** is shown in Figure 3b and the DSC data for all other compounds is included in the Supporting Information. The phase transition temperatures of compounds **3a**−**f** are summarized in Figure 3c. Structurally related compounds display the following three thermal features in a DSC trace.[36−43] Starting from a cooled sample, a sharp endothermic peak attributed to the crystalline to rectangular columnar mesophase (Cr→Col_r) occurs at low temperatures. Second, a weak endothermic mesophase-to-mesophase transition occurs, which is assigned to a transition to a hexagonal columnar (Col_h) phase, and finally the sharp endothermic transition from the Col_h to the isotropic liquid (Col_h→I) phase. The Cr→Col_r and Col_h→I transitions typically display small hysteresis, whereas the mesophase to mesophase (Col_r→Col_h) transitions exhibit large hysteresis.

Figure 3b shows the DSC trace of compounds **3a** upon heating and cooling. During the heating cycle from −50 °C, the di-*tert*-butyl derivative **3a** exhibits a large endothermic transition at −8 °C followed by a smaller, broad endothermic transition at 81 °C and a final sharp endothermic transition at 134 °C. The first endothermic transition at −8 °C for **3a** is consistent with a

crystalline to mesophase transition. Together with the room temperature XRD pattern, the mesophase can more accurately be described as a columnar rectangular phase (Col_r). Moreover, the Cr→Col_r phase transition is present in related compounds in a similar temperature range.[36−43] Compound **3a** is the only compound that is not near a phase transition at room temperature, which allows the assignment of the red bar in Figure 3c as the rectangular columnar phase. The second smaller phase transition at 81 °C is consistent with a rectangular to hexagonal (Col_r→Col_h) columnar phase transition, which is based on related compounds and is shown as the blue bar in Figure 3c. The final large endothermic phase transition at 134 °C is assigned to the hexagonal columnar to isotropic liquid (Col_h→I) phase transition. The indexing of the peaks for rectangular columnar phase was based on the report from Sun and co-workers.[56] The correlation length calculated from the full-width at half-maximum (fwhm) of the core-to-core peak for **3a** is large at 188 Å, which corresponds to 55 nearest neighbors in crystalline order. A large correlation distance is a feature that can be exploited in devices for one-dimensional charge transport. Most of the compounds studied here, except **3e**, show similar correlation lengths. The DSC traces for **3b**−**d** and **3f** exhibit similar phase transitions, except the Cr→Col is not observed above −50 °C, which is the limit of the instrument.

The ditolyl derivative **3b** shows a weak transition at 19 °C with a sharp transition at 136 °C. Clearly, the transition at 136 °C is consistent with the mesophase to isotropic liquid phase transition and the integrated area of the transition at 19 °C is consistent with a mesophase to mesophase transition. However, the mesophase to mesophase transition temperatures should be interpreted cautiously because previous work of He, Zhao, and Caille[60] has shown that the kinetics of phase reorganization plays a critical role in hysteresis and is dependent on thermal equilibration time and heating rate. Both compounds **3b** and **3c** display the typical diffraction pattern ascribed to the Col_h phase and provide the structural detail necessary to assign the phase in the DSC trace of Figure 3c. The difference between **3b** and **3c** is a methyl substituent. Conversely to expectations, the lattice parameter for the dibenzyl derivative (**3c**) is larger than the lattice parameter for the ditolyl derivative (**3b**). In addition, the correlation length of **3c** is less than **3b**, indicating there are fewer attractive forces between aromatic cores in the benzyl case (**3c**), which can only be attributed to increased van der Waals interactions for the ditolyl derivative (**3b**). Nevertheless, the larger lattice parameter and smaller correlation length of **3c** is consistent with lower Col_h→isotopic liquid phase transition from DSC experiments.

Compounds **3d** and **3f** have XRD patterns consistent with a Col_r phase. However, the XRD for **3d** also shows diffraction peaks in the midangle range suggesting a possible 3-dimensionally ordered structure. Until a single phase structure can be acquired, the assignment of an alternate phase is not possible. However, employing only the low angle diffraction peaks, compound **3d** shows a Col_r phase. Similarly, the XRD data of anthraquinone **3f** supports a Col_r phase at room temperature and the only mesophase-mesophase transition appeared at −25 °C, thus the phase at less than −25 °C remains unassigned.

Anthraquinone **3e** has a more complex XRD pattern at room temperature, which is consistent with a Col_h phase in the low angle region. However, there are also several additional *d*-spacing peaks that indicate the structure is more likely a 3-dimensional ordered phase. Until a single phase material can be formed, the absolute assignment of phase cannot be made. Nevertheless, using the low angle peaks of the XRD pattern a tentative assignment of Col_h phase is made. In addition, the DSC trace for anthraquinone **3e** shows transitions, which could be attributed to glass transitions.

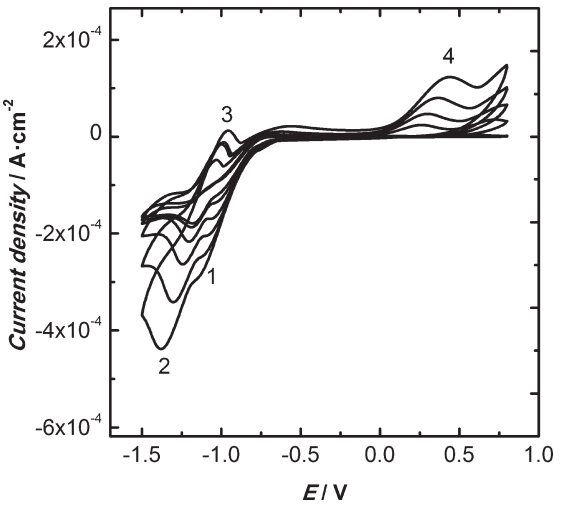

Figure 4. Cyclic voltammagram of 1.4 mM **3b** in THF containing 0.1 M $(n\text{-Bu})_4NPF_6$ at scan rates of 10, 20, 50, 100, 200, and 500 $mV \cdot s^{-1}$ at a glassy carbon working electrode and a Ag|AgCl|KCl_{3M} reference electrode.

Clearly, the LC thermal stability window is enhanced with pi-extended aromatic groups in the 1,5-positions. The thermal properties of **3a**−**f** indicate a useful temperature stability window, especially considering this class of material as *n*-type organic semiconductors for solar cell applications. Typical photovoltaic cell operating temperatures can reach 80 °C[61], and these compounds retain their LC properties at such temperatures. More importantly, the operating temperature stability window is dictated by small perturbations in long-range packing due to modest changes in organic structure, which opens the possibility to tune the organic materials to the application requirements in a simple, modular manner.

The electrochemical properties of AQs **2** and series **3** were determined by cyclic voltammetry (CV). The CV of **3b** is shown in Figure 4. In general, each of the AQ derivatives shows similar redox behavior and the similarities within AQ series **3** is discussed below. Typically, under aprotic, dry conditions AQs undergo two successive one-electron reductions to the radical anion and then to the dianion, shown by eqs 1 and 2.[62,63] The synthesized AQs are quite electron-rich owing to the installation of six alkoxy groups, resulting in a class of compounds that requires large negative potentials to be reduced. In the case of dihydroxy-AQ **2**, shown in the Supporting Information, the reduction peak occurs at −1.3 V vs Fc/Fc^+ and manifests as a single reduction wave attributed to a two-electron reduction (eqs 1 and 2).

$$AQ \underset{-e^-}{\overset{+e^-}{\rightleftharpoons}} AQ^- \quad (1)$$

$$AQ^- \underset{-e^-}{\overset{+e^-}{\rightleftharpoons}} AQ^{2-} \quad (2)$$

$$2AQ^- \rightleftharpoons AQ + AQ^{2-} \quad (3)$$

(60) He, Z.; Zhao, Y.; Caille, A. *Liq. Cryst.* **1997**, *23*, 317–325.

(61) Wang, D. H.; Im, S. H.; Lee, H. K.; Park, O. O.; Park, J. H. *J. Phys. Chem. C* **2009**, *113*, 17268–17273.

(62) Bauscher, M.; Mantele, W. *J. Phys. Chem.* **1992**, *96*, 11101–11108.

(63) Gupta, N.; Linschitz, H. *J. Am. Chem. Soc.* **1997**, *119*, 6384–6391.

Table 2. Summary of Electrochemical Results

compound	$E_{1/2}$[a](V)	D_O[b](10^{-6} cm$^2\cdot$s^{-1})	k_{et} (10^{-3} cm$\cdot$s^{-1})
3a	−1.587	4.0	1.6
3b	−1.594	7.3	2.2
3c	−1.703	6.1	1.8
3d	−1.544	1.4	0.9
3e	−1.530	0.4	5.2
3f	−1.524	3.0	1.2

[a] Reported potentials are referenced to Fc/Fc^+. [b] Calculated values assume oxidized diffusion coefficient (D_O) is equal to the reduced diffusion coefficient (D_R).

The return oxidation peak of AQ **2** is quasireversible with a peak separation of 300 mV at 500 mV$\cdot$s^{-1}. The CV for AQ **2** was carried out in dry acetonitrile at 45 °C to enhance the limited solubility and open the electrochemically accessible potential window. On the first cycle starting at 0 V and scanning anodically, there are no oxidation peaks as expected; however, after the reduction wave, two oxidation peaks are observed. The first oxidation peak is attributed to the reverse reaction of eqs 1 and 2. The second oxidation wave, which is only observed at scan rates >500 mV$\cdot$s^{-1}, is attributed to either an ion-pair between the electrolyte cation and the radical anion or to a protonated radical anion, which could arise from adventitious water.[64−69] For AQ series **3**, two reduction peaks, which are typically well separated in underivatized AQ, are labeled as shoulder 1 and peak 2 in Figure 4. The first reduction shoulder 1 (forward direction of eq 1) to the radical anion requires reductive potentials around −1.0 V. Peak 2 is attributed to the further one-electron reduction of the radical anion to the dianionic species (forward direction of eq 2). On the return anodic scan, two peaks are evident, labeled as peak 3 and peak 4 of Figure 4. Peak 3 is assigned to the return oxidation of the AQ dianion to the AQ radical anion (reverse direction of eq 2), and the $E_{1/2}$ values are reported in Table 2 for all compounds. Peak 4 is unusual because it is so anodically shifted, but its appearance was found in each AQ derivative synthesized. Peak 4 is attributed to a stabilized AQ radical anion, which could result from either an ion-pairing interaction or a protonated AQ radical anion.[64−69] Reversal of the scanning direction after shoulder 1 results in the growth of peak 4 at a sweep rate of 50 mV$\cdot$s^{-1}. An expansion of the slow scan rate in Figure 4 is included in the Supporting Information to highlight different redox behavior at scan rates <50 mV$\cdot$s^{-1}. At slow scan rates the same two reduction features (peak 1 and 2) are observed but the return oxidation potentials reveal no oxidation peaks, suggesting the formation of an electrochemically inactive species. For CVs with scan rates >50 mV$\cdot$s^{-1} the integration of all peaks shows charge balance between the sum of peaks 1 and 2 with peaks 3 and 4, suggesting the formation of the electrochemically inactive species is very slow, and this pathway is minimized at higher scan rates. CVs for compounds **3a**, **3c**−**e** also display an additional broad peak immediately following peak 3 in an anodic scan. This broad peak after peak 3 is attributed to the reoxidation of radical anion (nonstabilized) to the neutral AQ (reverse of eq 1). Note there are other equilibria to consider. The integration of peak 2 does not equal the charge consumed in peak 3, suggesting that the dianion has reacted to form a different chemical species. In quinone redox reactions, disproportionation (eq 3) and comproportionation (reverse of eq 3) reactions have been observed.[70,71] We propose that upon formation of the AQ dianion at scan rates >50 mV$\cdot$s^{-1}, a portion of the AQ dianions undergo a comproportionation reaction to form AQ radical anions. In the case of **3b**, the dianion is formed as shown by peak 2 of Figure 4 and then some of this dianion undergoes a comproportionation reaction to yield the AQ radical anion. The portion of AQ dianions that did not undergo the comproportionation are then reduced to the AQ radical anions in peak 3, which explains the unequal charge balance between peak 2 and 3. For **3b**, the majority of AQ radical anions that form in the cathodic scan are stabilized either by ion-pairing or water because of the absence of an oxidative wave immediately following peak 3. The stabilized AQ radical anions are then quantitatively oxidized to neutral AQ at peak 4. A CV of **3c** was carried out in acetonitrile and is included in the Supporting Information to expand the potential window and verify the charge balance. The CV in CH_3CN results in the two reductive peaks 1 and 2 and only the oxidation reaction at peak 4. In polar solvents, the comproportionation reaction is favored and the AQ radical anion is found exclusively in its stabilized form, as evidenced by the lack of peak 3 and presence of peak 4. Additionally, the integration of the background-subtracted current trace for peaks 1 and 2 are approximately equal to the charge passed in peak 4, implying charge balance and no electrochemically inactive species are formed. The redox potentials, $E_{1/2}$, of eq 2 for **3a**−**f** range from −1.52 to −1.70 V (vs Fc/Fc^+). **3a** and **3b**, with electron donating groups appended to the benzyl, exhibit the same redox potential, whereas the dibenzyl derivative **3c** is more difficult to reduce at −1.7 V. These redox potentials suggest the benzyl derivative is able to donate more electron density to the AQ, which could imply a more planar dibenzyl structure is adopted for **3c**. The addition of bulk to the 1,5-dibenzyl positions increases the intermolecular interactions which stabilizes the mesophase. The electron withdrawing groups (**3d** and **3e**) are easier to reduce than **1c** by ∼160 mV, as expected. Interestingly, the 1,5-dinaphthyl derivative **3f** shows a redox potential consistent with an electron withdrawing group. The anodically shifted redox potential of **3f**, suggests a strong intramolecular interaction between the naphthyl group and the electron rich AQ. It is possible that this interaction could be responsible for the high stability of the Col_r phase observed in the DSC trace for **3f**.

The quasireversible redox peaks (2 and 3 of Figure 4) are represented by eq 2 and the electron transfer rates can be quantified by using the method reported by Nicholson.[72] First, a determination of diffusion coefficient is needed, which is determined by plotting the peak current as a function of square root of scan rate, according to the Randles−Sevcik[73] equation. The linear relationship between square root of the scan rate and peak current is critical to qualify these compounds as operating under diffusion control. Note that only scan rates between 50 and 1000 mV$\cdot$s^{-1} were used and showed a linear relationship with R^2 values >0.96, which is important considering the propensity of these compounds to form films and aggregate structures, which would result in deviations from linearity. Assuming the diffusion coefficient of the reduced species is equal to the diffusion coefficient of the oxidized species and the transfer coefficient is 0.5, provides the basis to use Nicholson's method in determining the heterogeneous electron transfer rate constant. Both the diffusion coefficients and rate constants are included in Table 2. Diffusion

(64) Bessard, J.; Cauquis, G.; Serve, D. *Electrochim. Acta* **1980**, *25*, 1187–1197.
(65) Eggins, B. R. *J. Chem. Soc., D* **1969**, 1267–1268.
(66) Eggins, B. R.; Chambers, J. Q. *Chem. Commun.* **1969**, 232–233.
(67) Khalid, I. M.; Alvarez, J. C. *J. Electroanal. Chem.* **2009**, *631*, 76–79.
(68) Lehmann, M. W.; Evans, D. H. *J. Phys. Chem. B* **2001**, *105*, 8877–8884.
(69) Tabakovic, I.; Davidovic, A.; Mueller, W. E. G.; Zahn, R. K.; Sladic, D.; Dogovic, N.; Gasic, M. J. *Bioelectrochem. Bioenerg.* **1987**, *17*, 567–577.
(70) Roginsky, V. A.; Pisarenko, L. M.; Bors, W.; Michel, C. *J. Chem. Soc., Perkin Trans. 2* **1999**, 871–876.
(71) Song, Y.; Buettner, G. R.; Parkin, S.; Wagner, B. A.; Robertson, L. W.; Lehmler, H. J. *J. Org. Chem.* **2008**, *73*, 8296–8304.
(72) Nicholson, R. S. *Anal. Chem.* **1965**, *37*, 1351–1355.
(73) Bard, A. J.; Faulkner, L. R. *Electrochemical methods: fundamentals and Applications*, 2nd ed.; Wiley: New York, 2001; p xxi, 833.

coefficients are typical for molecules of this size and range from 3.5×10^{-7} to 7.3×10^{-6} $cm^2 \cdot s^{-1}$. The electron transfer rate constants associated with eq 2 reaction are tabulated in Table 1 and range from 0.9 to 5.2×10^{-3} $cm \cdot s^{-1}$. These electron transfer rates are not considered fast, but since the rates are solution-based these compounds warrant future investigation as possible *n*-type conductors.

Conclusion

This contribution shows a convenient path to the synthesis of anthraquinone LC compounds using microwave synthesis. UV−vis absorption profiles show that the anthraquinone is the chromophore with little electronic perturbation derived from the benzyl substituents and the compounds have a large HOMO−LUMO energy gap, which is acceptable as an *n*-type component in organic materials. The thermal phase properties of compounds **3a**−**f**, X-ray diffraction data, and the cross-polarized microscopy results indicate these AQs form discotic columnar phases that exhibit a thermal stability window that spans 175 °C. XRD experiments show all of the compounds synthesized display columnar discotic structures at room temperature and are classified as either rectangular or hexagonal columnar phases. The large, tunable LC temperature stability window is relevant to organic photovoltaic applications. Solution electrochemical results indicate a reasonable reduction potential for *n*-type materials and electron transfer kinetics that do not preclude these materials from further device investigation. However, a lower reduction potential and faster electron transfer rates would be beneficial, and current efforts are directed at the synthesis of compounds that exhibit faster charge transfer leading to better solid-state conductance.

Experimental Section

Synthesis. Solvent were dried using an MBraun solvent system. ^{1}H- and ^{13}C{^{1}H}-NMR spectra were recorded on a Bruker DMX-300 or a Bruker DRX-400 spectrometer. Elemental analyses were performed at the University of Calgary, Department of Chemistry. Mass spectrometry was carried out using a Finigan SSQ700 spectrometer. Differential scanning calorimetry was carried out using TA Instruments Q200 instrument scanning from −50 to 200 °C at a rate of 10 °C·min^{-1}. UV−vis−NIR spectra were recorded in dry THF solutions in a 1 cm quartz cell on a Cary5000 spectrometer.

***1**: Rufigallol, 1,2,3,5,6,7-Hexahydroxyanthracene-9,10-dione*. The acid-mediated self-condensation of Gallic acid was facilitated under microwave conditions using a previously reported procedure and gave Rufigallol in 78−84% yield.[43] Gallic acid (0.48 g, 2.8 mmol) was dissolved completely in 98% sulfuric acid (5 mL). The vial was capped with a vented rubber septum and heated by conventional microwave oven for 5 s, with ∼1 min breaks in between each heating cycle for a total of 45 s. During the microwave reaction, the color of the solution changed from amber to purple. Once the reaction was complete, the sample was poured into a beaker of ice−water, and the brick red precipitate was filtered resulting in crude rufigallol (0.32 g, 1.1 mmol, 78%).

***2**: 2,3,6,7-Tetrakis(dodecyloxy)-1,5-dihydroxyanthracene-9,10-dione*. Crude rufigallol **1** (0.70 g, 2.3 mmol) was tetraalkylated in the 2,3,6,7-hydroxy positions by stirring with sodium hydroxide (0.40 g, 9.9 mmol) and TBAB (3.20 g, 10.0 mmol) in DMSO (14 mL) at room temperature (15 min) under inert conditions. Upon addition of 1-bromododecane (2.6 mL, 2.7 g, 10.8 mmol), the sample was heated to 85 °C for 18 h. The reaction mixture was cooled to room temperature, and water (6 mL) was added to precipitate the product. The crude product was filtered from the reaction mixture and dissolved in chloroform (50 mL), which was then extracted with water (3 × 200 mL) and brine (200 mL). After two recrystallizations from chloroform and methanol, yellow powder tetraether was obtained in 40% yield (0.90 g, 0.92 mmol). ^{1}H NMR (300 MHz, $CDCl_3$): δ 12.78 (s, 1H), 7.42 (s, 1H), 4.17 (t, J = 6.7 Hz, 2H), 4.15 (t, J = 6.6 Hz, 2H), 2.02−1.64 (m, 4H), 1.66−0.95 (m, 42H), 0.88 (t, J = 6.6 Hz, 6H).

General Procedure for Hexaether Synthesis. Compound **2** (typically 0.2 g, 0.2 mmol) was dialkylated at the 1,5-hydroxy positions by stirring with potassium carbonate (0.20 g, 1.4 mmol), TBAB (0.11 g, 0.33 mmol), and DMF (10 mL) at room temperature (15 min) under inert conditions. The appropriate benzylbromide derivative was added (approximately 3.5 mmol), and the flask was heated to 105 °C for 20 h. The reaction mixture was cooled to room temperature and water (10 mL) was added to precipitate the product. The crude product was filtered from the reaction mixture and dissolved in chloroform (50 mL), which was extracted with water (3 × 200 mL) and brine (200 mL). After two precipitations from mixed solvents, chloroform and ethanol, clean yellow waxy hexaethers were obtained in 65−92% yields (approximately 0.20 mmol).

***3a**: 1,5-Bis(4-(t-butyl)benzyloxy)-2,3,6,7-tetradodecyloxyanthracene-9,10-dione*. Compound **2** (0.20 g, 0.20 mmol), and 4-(*tert*-butyl)benzyl bromide (0.5 mL, 0.62 g, 2.2 mmol) were reacted according to the general procedure for hexaether synthesis. The product was a waxy yellow solid (0.22 g, 0.17 mmol, 83%). ^{1}H NMR (300 MHz, $CDCl_3$): δ 7.90−7.56 (m, 3H), 7.46 (d, J = 8.2 Hz, 2H), 5.10 (s, 2H), 4.20 (t, J = 6.4 Hz, 2H), 4.10 (t, J = 6.5 Hz, 2H), 2.17 (s, 1H), 2.03 − 1.65 (m, 4H), 1.64−1.14 (m, 45H), 0.90 (t, J = 6.6 Hz, 6H). ^{13}C NMR (75 MHz, $CDCl_3$): δ 181.21, 157.52, 153.24, 150.98, 147.28, 134.49, 132.73, 128.76, 125.37, 120.86, 107.40, 77.36, 75.64, 74.32, 69.26, 34.67, 32.05, 31.48, 30.48, 29.85, 29.82, 29.78, 29.74, 29.65, 29.49, 29.22, 26.19, 22.81, 14.22. MS (Supporting Information) *m*/*e* calcd for $C_{84}H_{132}O_8$ (100, M + Na^+), 1291.98; found, 1291.79. Anal. Calcd for $C_{84}H_{132}O_8$: C, 79.44; H, 10.48; N: 0. Found: C, 79.14; H, 10.37; N, 0.11.

***3b**: 1,5-Bis(4-(methyl)benzyloxy)-2,3,6,7-tetradodecyloxyanthracene-9,10-dione*. Compound **2** (0.21 g, 0.21 mmol), and 4-(methyl)benzyl bromide (0.62 g, 3.4 mmol) were reacted according to the general procedure for hexaether synthesis. The product was a waxy, yellow-brown solid (0.23 g, 0.19 mmol, 90%). ^{1}H NMR (300 MHz, $CDCl_3$): δ 7.99−7.42 (m, 3H), 7.22 (m, 2H), 5.07 (s, 2H), 4.18 (t, J = 6.3 Hz, 2H), 4.06 (t, J = 6.5 Hz, 2H), 2.37 (s, 3H), 2.14−1.64 (m, 4H), 1.64−0.97 (m, 36H), 0.88 (t, J = 6.6 Hz, 6H). ^{13}C NMR (75 MHz, $CDCl_3$): δ 181.25, 157.54, 153.27, 147.26, 137.73, 134.53, 132.73, 129.12, 128.93, 120.82, 107.40, 77.58, 77.16, 76.74, 75.71, 74.32, 69.29, 32.05, 30.47, 29.85, 29.82, 29.78, 29.75, 29.65, 29.49, 29.22, 26.17, 22.81, 21.38, 14.23. MS-(Supporting Information) *m*/*e* calcd for $C_{78}H_{120}O_8$ (100, M + Na^+), 1207.89; found, 1207.63. Anal. Calcd for $C_{78}H_{120}O_8$: C, 79.01; H, 10.20. Found: C, 78.48; H, 10.08.

***3c**: 1,5-Bis(benzyloxy)-2,3,6,7-tetradodecyloxyanthracene-9,10-dione*. Compound **2** (0.10, 0.10 mmol), and benzyl bromide (0.3 mL, 0.43 g, 2.5 mmol) were reacted according to the general procedure for hexaether synthesis. The product was a waxy, yellow solid (0.093 g, 0.080 mmol, 78%). ^{1}H NMR (300 MHz, $CDCl_3$) δ 7.79−7.53 (m, 3H), 7.56−7.28 (m, 3H), 5.12 (s, 2H), 4.19 (t, J = 6.4 Hz, 2H), 4.08 (t, J = 6.5 Hz, 2H), 2.04−1.81 (m, 2H), 1.81−1.63 (m, 2H), 1.63−1.10 (m, 37H), 0.88 (t, J = 6.6 Hz, 6H). ^{13}C NMR (75 MHz, $CDCl_3$): δ 181.26, 157.63, 153.27, 147.33, 137.58, 132.77, 128.85, 128.48, 128.10, 120.76, 107.48, 75.79, 74.38, 69.32, 32.06, 30.47, 29.83, 29.80, 29.76, 29.63, 29.50, 29.22, 26.19, 22.82, 14.24. MS (Supporting Information) *m*/*e* calcd for $C_{76}H_{116}O_8$ (100, M + H^+), 1157.87; found, 1157.90. Anal. Calcd for $C_{76}H_{116}O_8$: C, 78.85; H, 10.10; N, 0. Found: C, 78.16; H, 9.95; N, 0.07.

***3d**: 1,5-Bis(4-(bromo)benzyloxy)-2,3,6,7-tetradodecyloxyanthracene-9,10-dione*. Compound **2** (0.09 g, 0.092 mmol), and 4-(bromo)benzyl bromide (0.30 g, 1.2 mmol) were reacted according to the general procedure for hexaether synthesis. The product

was a light yellow solid (0.083 g, 0.063 mmol, 69%). ^{1}H NMR (300 MHz, $CDCl_3$): δ 7.77−7.45 (m, 5H), 5.06 (s, 2H), 4.18 (t, J = 6.3 Hz, 2H), 4.06 (t, J = 6.5 Hz, 2H), 2.06−1.80 (m, 2H), 1.80−1.63 (m, 2H), 1.63−0.99 (m, 37H), 0.88 (t, J = 6.5 Hz, 6H). ^{13}C NMR (75 MHz, $CDCl_3$): δ 181.26, 157.68, 152.98, 147.24, 136.58, 132.66, 131.62, 130.40, 122.13, 120.66, 107.59, 74.91, 74.44, 69.40, 32.07, 30.49, 29.87, 29.83, 29.80, 29.77, 29.76, 29.65, 29.53, 29.51, 29.22, 26.19, 22.84, 14.27. MS (Supporting Information) *m*/*e* calcd for $C_{76}H_{114}Br_2O_8$ (100, M + Na^+), 1337.68; found, 1337.61. Anal. Calcd for $C_{76}H_{114}Br_2O_8$: C, 69.39; H, 8.73; N, 0. Found: C, 69.09; H, 8.78; N, −0.03.

***3e**: 1,5-Bis(4-(trifluoromethyl)benzyloxy)-2,3,6,7-tetradodecyloxyanthracene-9,10-dione*. Compound **2** (0.20 g, 0.21 mmol), and 4-(trifluoromethyl)benzyl bromide (0.65 g, 2.7 mmol) were reacted according to the general procedure for hexaether synthesis. The product was a light yellow solid (0.17 g, 0.13 mmol, 64%). ^{1}H NMR (300 MHz, $CDCl_3$): δ 7.80 (d, J = 8.1 Hz, 2H), 7.75−7.59 (m, 3H), 5.17 (s, 2H), 4.18 (t, J = 6.3 Hz, 2H), 4.07 (t, J = 6.5 Hz, 2H), 1.97−1.81 (m, 2H), 1.81−1.63 (m, 2H), 1.63−1.07 (m, 38H), 0.88 (t, J = 6.6 Hz, 6H). ^{13}C NMR (75 MHz, $CDCl_3$): δ 181.17, 157.74, 152.93, 147.26, 141.65, 132.64, 128.49, 125.49, 125.44, 120.59, 107.67, 74.71, 74.50, 69.44, 32.07, 30.48, 29.84, 29.81, 29.77, 29.62, 29.51, 29.22, 26.19, 22.84, 14.25. MS (Supporting Information) *m*/*e* calcd for $C_{78}H_{114}F_6O_8$ (100, M + Na^+), 1315.83; found, 1315.96. Anal. Calcd for $C_{78}H_{114}F_6O_8$: C,72.41; H, 8.88; N, 0. Found: C, 72.39; H, 8.73; N, 0.05.

***3f**: 1,5-Bis(naphthyloxy)-2,3,6,7-tetradodecyloxyanthracene-9,10-dione*. Compound **2** (0.12, 0.12 mmol), and 2-(bromomethyl)naphthalene (0.34 g, 1.5 mmol) were reacted according to the general procedure for hexaether synthesis. The product was a waxy, yellow solid (0.12 g, 0.097 mmol, 79%). ^{1}H NMR (300 MHz, $CDCl_3$): δ 8.10 (s, 1H), 8.01−7.75 (m, 4H), 7.67 (s, 1H), 7.50 (dd, J = 6.1, 3.2 Hz, 2H), 5.31 (s, 2H), 4.16 (t, J = 6.3 Hz, 2H), 4.05 (t, J = 6.5 Hz, 2H), 2.01−1.79 (m, 2H), 1.79−1.62 (m,2H), 1.64−1.02 (m, 36H), 0.90 (t, J = 6.4 Hz, 6H). ^{13}C NMR (75 MHz, $CDCl_3$): δ 181.38, 157.67, 153.30, 147.31, 135.14, 133.51, 133.35, 132.74, 128.26, 128.19, 127.82, 127.48, 126.72, 126.03, 120.86, 107.56, 104.70, 75.94, 74.47, 69.35, 32.07, 30.52, 29.85, 29.81, 29.78, 29.66, 29.52, 29.24, 26.20, 22.84, 14.27. MS (Supporting Information) *m*/*e* calcd for $C_{84}H_{120}O_8$ (100, M + Na^+), 1279.89; found, 1279.65. Anal. Calcd for $C_{84}H_{120}O_8$: C, 80.21; H, 9.62; N, 0. Found: C, 79.80; H, 9.48, N: 0.06.

Electrochemistry. Dry THF (inhibitor free) from an MBraun solvent system was used to make a 0.1 M electrolyte solution from electrochemical grade tetra-*n*-butylammonium hexafluorophosphate (Fluka). Electrochemical solutions were purged with Ar for 20 min in a conventional three-electrode, temperature-controlled cell. The working electrode was a carbon disk (geometric area = 0.28 cm^2) that was polished with alumina (0.05 μm) slurry, briefly sonicated in EtOH, and rinsed with excessive amounts of THF prior to each measurement. The counter-electrode was a Pt wire that was flame annealed prior to each experiment, and the reference electrode was a commercial Ag|AgCl|KCl_{3M} electrode (Bioanalytical Systems, Inc.). Cyclic voltammetry experiments were conducting using a commercial potentiostat (AutoLab PGSTAT302), and data acquisition was controlled through software interface (GPES 4.9).

Acknowledgment. The authors thank the Natural Sciences and Engineering Research Council of Canada, Alberta Government, Canadian Foundation for Innovation and the Institute for Sustainable Energy, Environment and Economy for funding. The authors also thank V. Thangadurai for discussions and use of the XRD instrument.

Supporting Information Available: Table of DSC transition temperatures; cyclic voltammagrams of supporting electrolyte in THF, **2**, **3a**, **3c**−**f**; DSC traces of **3c**−**f**; XRD of **3a**−**f** and ^{1}H and ^{13}C NMR spectra of **3a**−**f**. This material is available free of charge via the Internet at http://pubs.acs.org.